(Preprint) AAS XX-XXX

ANALYSIS AND OPTIMIZATION OF ROBUST TRAJECTORIES IN CISLUNAR ENVIRONMENT WITH APPLICATION TO THE LUMIO CUBESAT

Carmine Giordano[*], and Francesco Topputo[†]

Nowadays, the space exploration is going in the direction of exploiting small platforms to get high scientific return at significantly lower costs. However, miniaturized spacecraft pose different challenges both from the technological and mission analysis point of view. While the former is in constant evolution due to the manufacturers, the latter is an open point, since it is still based on a traditional approach, not able to cope with the new platforms' peculiarities. In this work, a revised preliminary mission analysis approach, merging the nominal trajectory optimization with a complete navigation assessment, is formulated in a general form and three main blocks composing it are identified. Then the integrated approach is specialized for the transfer trajectory of the LUMIO CubeSat, showing the advantage of this methodology for miniaturized platforms in a chaotic environment.

INTRODUCTION

Since the beginning of the space era, satellites have always been equipped with chemical propulsion engines, characterized by a high value of thrust and a good control authority. For traditional spacecraft, nominal trajectories are designed and optimized in order to satisfy only scientific requirements as well as to comply with system constraints. Although, the nominal path will unlikely be followed by the spacecraft in real-life scenarios due to uncertainty in *dynamic model* (e.g., gravitational parameters or radiation pressure noisy profiles), *navigation* (i.e. imperfect state knowledge or approximations in measurement model), and *command actuation* (i.e., thrust magnitude and pointing angles error),[1] the correction maneuvers needed to compensate deviations are considered to be a minor problem, since changing the trajectory is relatively easy with a single, short burn. Robustness and feasibility assessment of the nominal trajectory against uncertainty are performed a-posteriori through a navigation analysis, with the aim to perform a covariance analysis and compute the achievable state knowledge, and to estimate the correction maneuvers. Thus, the nominal trajectory and the uncertainty assessment are decoupled and their analysis and optimization are done in two separate phases. This approach can lead to sub-optimal solutions. For large spacecraft, this procedure is acceptable since they can produce high thrust levels and they can store relevant propellant quantities; hence, sub-optimal trajectories are not critical.

However, in recent times, the space exploration is going in the direction of exploiting small platforms, such as SmallSat or CubeSat, in order to get scientific and technological return at significantly lower costs.[2,3] In this kind of probes, the low control authority poses challenges in maneuvering,

[*]PostDoc Fellow, Department of Aerospace Science and Technology, Politecnico di Milano, via La Masa, 34, Milan, 20156, Italy.

[†]Full Professor, Department of Aerospace Science and Technology, Politecnico di Milano, via La Masa, 34, Milan, 20156, Italy.

since a long burn is needed, even for paltry deviations. Therefore, orbit determination and the subsequent correction maneuvers cannot be considered a minor problem and preliminary trajectory design should take them into account.
A clear indication of this phenomenon can already be found in missions exploring small satellites, as Lisa PathFinder (LPF) proposed mission extension,[4] where the best solution requires a deterministic $\Delta v = 0.657\,\mathrm{m/s}$, but the navigation Δv distribution for the given trajectory gives a value of $4.533\,\mathrm{m/s}$ for a 95% confidence level. A similar behavior can be found also in the LUMIO Phase 0 study.[5] In this case, the deterministic cost for the transfer amounts to $89.97\,\mathrm{m/s}$, while the 3σ stochastic cost sums up to $97.9\,\mathrm{m/s}$. Hence, the nominal and navigation Δvs have the same order of magnitude. In such cases, a procedure embedding uncertainty in the preliminary mission design can be useful in cutting down the overall mission costs and produce more robust and feasible solutions.
In the last decades, optimal control and optimization theory have been extensively exploited for the nominal design of space trajectories.[6,7] However, only in the last ten years, some stochastic-optimal approaches, embedding uncertainty in their core, have been developed.[8–12]
Although uncertainties in the early stages of the trajectory design are considered in recent works to devise robust optimal trajectories, an integrated approach, considering the navigation assessment as part of the trajectory design and optimization, using classical techniques, is still missing. Nevertheless, the paradigm shift proposed in this work can be beneficial in terms of propellant mass consumption. Indeed, it can overtake the natural sub-optimality of the traditional approach by surfing solutions with lower dispersion and better stochastic properties, thus reducing both the navigation costs and the final state scattering with respect to the target. Hence, robust low-cost trajectories in the preliminary mission analysis can increase the scientific return for small satellites either by giving access to nowadays-impossible mission profiles or by expanding the nominal operative life.

PROBLEM STATEMENT

Sequential Approach

In this work, the approach followed nowadays to compute a nominal trajectory, evaluate its statistical properties and retrieve the navigation costs is labeled as *sequential* or *traditional approach*. Detailed information about this process can be found in several sources.[5,13] In this case, the whole procedure is subdivided into two *sequential and independent steps* (Figure 1):

1. *Trajectory Design and Optimization*: nominal trajectory, connecting the initial point to the target, while minimizing the propellant mass, is sought (Figure 1a). Thus, generally speaking, an optimal control problem is set up, having the aim to determine the state $\mathbf{x}(t)$, the control $\mathbf{u}(t)$ and, possibly, the initial and final times, t_0 and t_f, that minimize the total control effort

$$J = \int_{t_0}^{t_f} \|\mathbf{u}\| \, \mathrm{d}t$$

subject to the ordinary differential equation

$$\dot{\mathbf{x}} = \mathbf{f}(\mathbf{x}, \mathbf{u}, t)$$

and to the boundary constraints

$$\mathbf{x}(t_0) = \mathbf{x}_0$$
$$\mathbf{x}(t_f) = \mathbf{x}_f$$

The function $\mathbf{f}$ represents the acceleration vector field associated to the spacecraft dynamics. Some additional terminal and path constraints are normally added, considering the characteristics of the specific orbital problem.

2. *Navigation Assessment*: the nominal trajectory "flyability" in a real scenario is evaluated by simulating the orbit determination (OD) process and estimating the trajectory correction maneuvers (TCM) along the whole mission. Thus, the Navigation Assessment can be split into two (independent) sub-phases: i. *Knowledge analysis*: a covariance analysis is performed to estimate the achievable level of accuracy in the spacecraft state *knowledge*; ii. *Navigation cost estimation*: a stochastic analysis is performed in order to estimate the navigation cost needed to allow the spacecraft to reach the target (Figure 1c), computing also the trajectory *dispersion*, i.e., the deviation of the true spacecraft state with respect to its nominal value. Knowledge analysis and navigation cost estimation are usually performed independently in the preliminary mission analysis. However, in principle, they cannot be considered totally separate: both sub-phases should share a common timeline and the navigation costs are dependent on the knowledge level.

Figure 2 shows the general architecture for the traditional approach.

Integrated Approach

A procedure able to comprehend the whole navigation assessment inside the optimization process has to be designed. This method will be tagged as *integrated* or *revised approach*. It aims to 1) evaluate and minimize deterministic and stochastic cost, 2) estimate the knowledge, 3) and compute the dispersion, at the same time. In order to achieve these objectives, the approach depicted in Figure 3 is devised. The initial nominal state is given together with the associated initial dispersion. For each state belonging to the initial dispersion, an initial knowledge is considered. These three quantities (nominal state, knowledge and dispersion) are propagated forward. At some prescribed times, an OD process is performed in order to estimate the true trajectory and reduce the knowledge covariance. The estimated trajectory is then used to feed a guidance scheme, compute the correction maneuver and reduce the dispersion. At the end, the final nominal state and the final dispersion can be retrieved. For sake of simplicity, considering a Monte Carlo fashion, the revised approach can be summarized as:

For each step of the optimization algorithm:

1. An initial nominal state $\mathbf{x}_0$ (blue dot in Figure 3) and initial dispersion (blue ellipse) are given;
2. The initial state is propagated up to the final time, in order to generate the nominal trajectory (black line) and compute the nominal cost;
3. A number of samples in the initial dispersion $\mathbf{x}_0^i$ (orange dot) are generated;
4. For each sample:
   (a) The initial state $\mathbf{x}_0^i$ and the associated initial knowledge are propagated forward (orange line) up to the first OD time;
   (b) In a give time span $t \in \left[t_0^{OD}, t_f^{OD}\right]$, the OD is performed (gray thick line) to improve the knowledge (black ellipses);

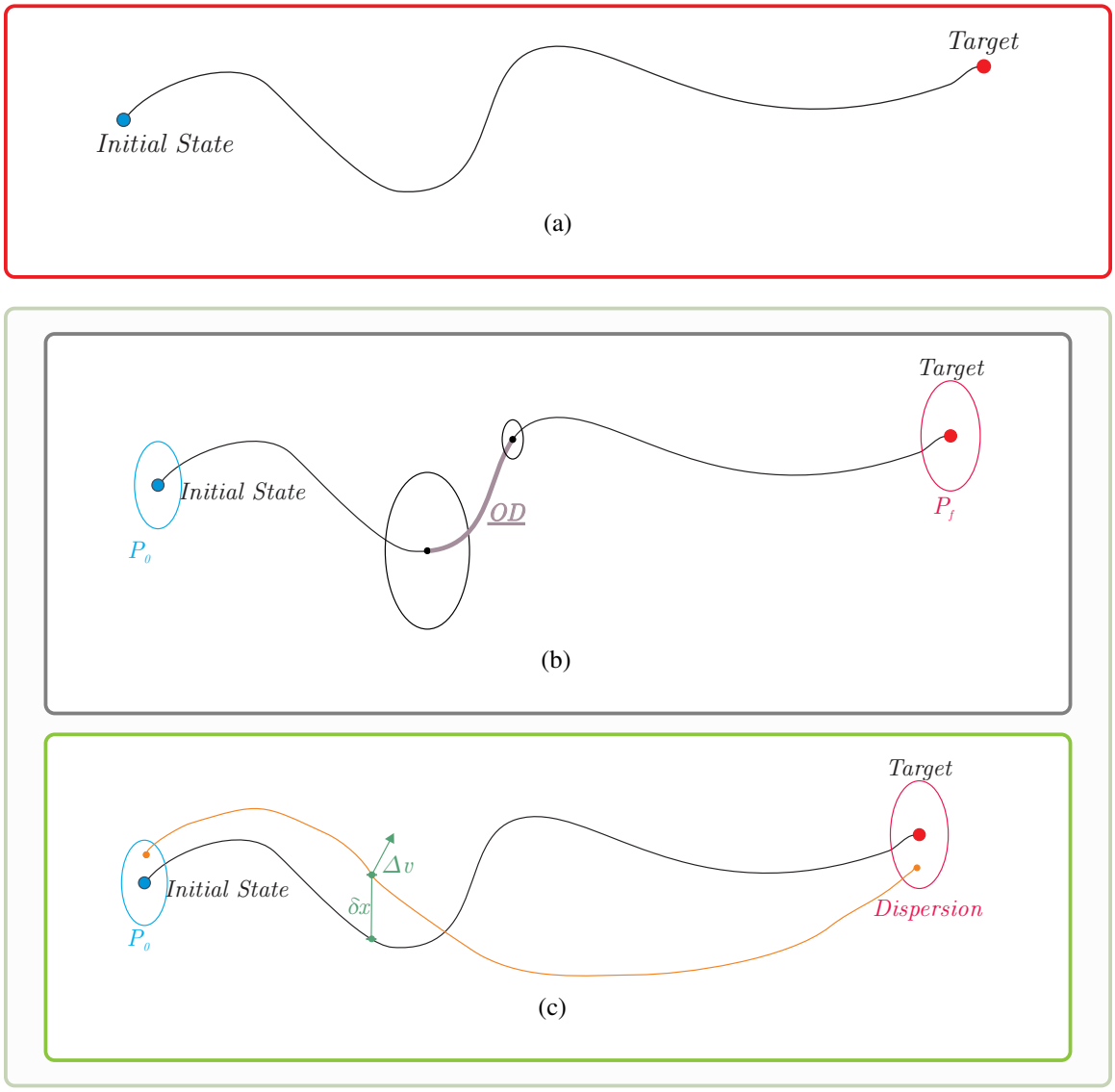

Figure 1: Traditional approach for preliminary mission analysis: (a) Trajectory design and optimization; (b) Knowledge analysis; (c) Navigation cost evaluation. Nominal trajectory is indicated with a black line, true trajectory as an orange line, OD with a grey thick line. Ellipses represent the instantaneous (b) knowledge (c) or dispersion. Steps (b)–(c) form the navigation assessment.

(c) An estimated state (magenta dot) is retrieved at the end of the OD and pushed forward in time, in order to compute the TCM (green arrow) through a guidance law;

(d) The real trajectory is propagated up to the correction maneuver time t_{TCM}, when the navigation impulse is applied;

(e) Steps 4a–4d are repeated for each OD and correction maneuver time up to the final time t_f.

5. From the Monte Carlo-like simulation, statistics for the navigation cost can be computed and the final dispersion (red ellipse) can be estimated.

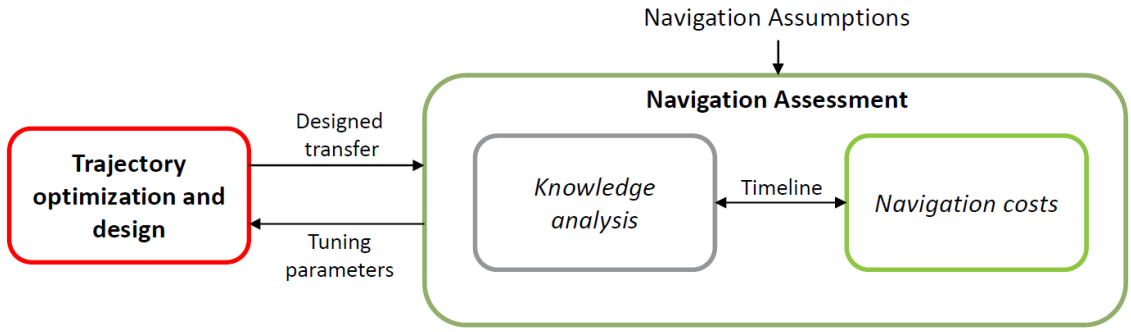

Figure 2: Traditional approach architecture

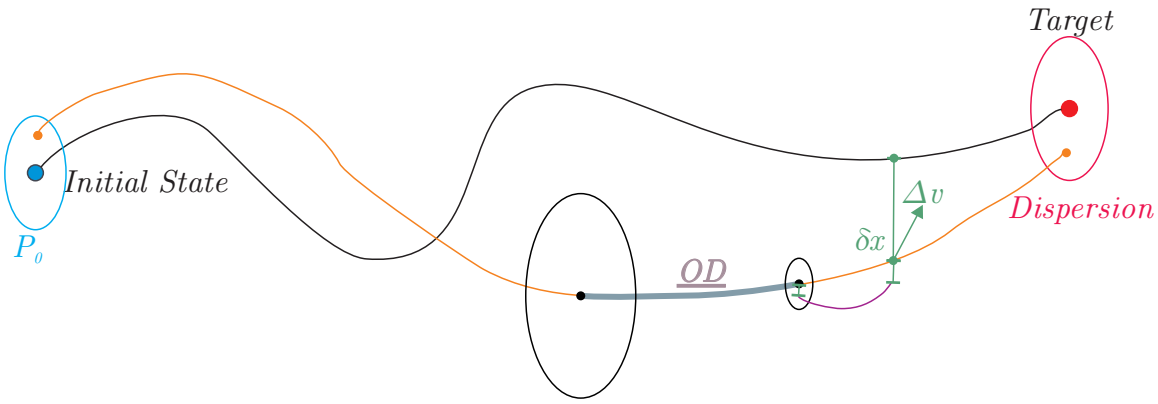

Figure 3: Revised approach for the preliminary mission analysis. Nominal trajectory is indicated with a black line, a true possible trajectory with an orange line, estimated trajectory with a magenta line. The OD process is the gray thick line. Black ellipses represent the instantaneous knowledge; colored ellipses represent the dispersion.

6. The total propellant mass, given by deterministic plus stochastic Δv is optimized, while imposing a constraint on the final state.

Generally speaking, the general fuel-optimal problem of a spacecraft flying in a perturbed environment under the revised approach can be formalized as:

Definition 1 (Fuel-Optimal General Problem) *Find the nominal state $\mathbf{x}^*(t)$, the nominal control history $\mathbf{u}^*(t)$ and, possibly, the initial and final times, t_0 and t_f, such that*

$$J = \int_{t_0}^{t_f} \|\mathbf{u}^*\| \, \mathrm{d}t + Q(\Delta v^s) \tag{1}$$

with $Q(\Delta v^s)$ a measure of the stochastic cost, is minimized, while the state is subjected to a simplified Itô stochastic differential equation[14]

$$\dot{\mathbf{x}} = \mathbf{f}\left(\mathbf{x}, \mathbf{u}, t\right) + \boldsymbol{\omega}\left(\mathbf{x}, \mathbf{u}, t\right) \tag{2}$$

with $\mathbf{f}$ being the deterministic part of the dynamics and $\boldsymbol{\omega}$ the process noise associated to uncertainty in dynamics and in maneuver execution.

Moreover, the state is subjected to initial constraints on dispersion

$$\begin{cases} E\left[\mathbf{x}^*(t_0)\right] = \mathbf{x}_0 \\ E\left[\left(\mathbf{x}^*(t_0) - \mathbf{x}_0\right)\left(\mathbf{x}^*(t_0) - \mathbf{x}_0\right)^T\right] = P_0^d \end{cases} \tag{3}$$

and on knowledge

$$E\left[\left(\mathbf{x}(t_0) - \mathbf{x}_0\right)\left(\mathbf{x}(t_0) - \mathbf{x}_0\right)^T\right] = P_0^k \tag{4}$$

and a final constraint

$$\mathcal{E}\left(\mathbf{x}\left(t_f\right), t_f\right) \subseteq \hat{\mathcal{E}}_\delta\left(t_f\right) \tag{5}$$

with $\mathcal{E}$ indicating a generalized uncertainty ellipsoid and $\hat{\mathcal{E}}_\delta$ the desired ellipsoid.
The navigation costs are estimated through a guidance law, fed by the OD scheme. It means

$$\Delta v^s = \texttt{GL}\left(\mathbf{x}^*, \hat{\mathbf{x}}, t_{TCM}\right) \tag{6}$$

and

$$\hat{\mathbf{x}}\left(t_f^{OD}\right) = \texttt{OD}\left(\mathbf{x}, \hat{\mathbf{x}}, t_0^{OD}, t_f^{OD}\right) \tag{7}$$

with GL *and* OD *being the guidance law and orbit determination procedures respectively, $\hat{\mathbf{x}}$ is the estimated state, $\mathbf{x}$ the real state and $\mathbf{x}^*$ is the nominal state.*

For the integrated approach, three main building blocks can be identified and they are: 1) a procedure to propagate uncertainty and to evaluate the stochastic measures, 2) a *OD scheme*, and 3) a *guidance law*, that can vary and should be selected properly, depending on the analyzed scenario.

TEST CASE SCENARIO

A comprehensive method for robust stochastic mission analysis seems to be unfeasible: deep-space exploration missions have diverse characteristics and mission profiles vary so widely that a single technique will be never able to produce a good solution for each situation. In fact, Problem 1 provides a general framework with its building blocks, that should be adapted to the scenario of interest. In this work, the LUMIO transfer phase, from a low lunar orbit (LLO) to a halo orbit, is considered. This scenario provides a relevant environment to test the revised approach and assess its performances.
LUMIO[15] is a 12U form-factor CubeSat, flying a halo orbit at Earth–Moon L_2. The spacecraft is equipped with the LUMIO-Cam, a novel miniaturized optical instrument capable of detecting light flashes in the visible spectrum produced by meteoroid impacts. Indeed, LUMIO shall observe, quantify, and characterize meteoroid impacts on the lunar farside by detecting their flashes, complementing Earth-based observations on the Lunar nearside, to provide global information on the lunar meteoroid environment and contribute to lunar situational awareness.[16] The whole mission profile is summarized in Figure 4. During the parking phase, LUMIO is released on a low lunar orbit by the carrier. A $600\,\mathrm{km} \times 20\,000\,\mathrm{km}$ LLO parking orbit is chosen out. Angular parameters are considered free to vary. LUMIO operative orbit is quasi-periodic halo orbit about Earth–Moon L_2 characterized by a Jacobi constant $C_j = 3.09$.[5] According to the timeline of the mission, defined during Phase A, the operative phase is expected to start on 21 March, 2024, and to end on 22 March, 2025. In this work, the operative orbit serves as a moving target on a prescribed trajectory.
During the transfer, LUMIO is brought from the low lunar orbit to the operative orbit. Free transport mechanisms are leveraged to reach the target halo. Specifically, intersection in the configuration

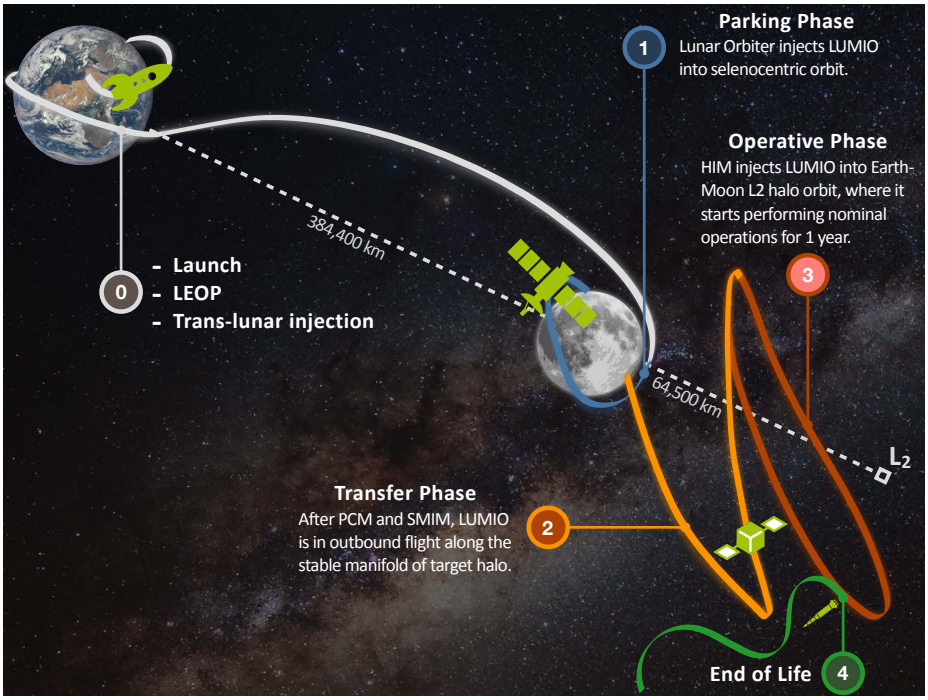

Figure 4: LUMIO mission profile (from[5]).

space has to be sought between the halo stable manifolds and a selenocentric transition orbit. Since the sought intersection occurs only in physical space, a maneuver is necessary for orbital continuity. This maneuver places the spacecraft on the stable manifold of the target halo and is thus called stable manifold injection maneuver (SMIM) and it will be indicated with Δv_{SMIM}. After the transfer, the halo injection maneuver (HIM), Δv_{HIM}, eventually injects the CubeSat into the final operative orbit. A detailed study of the TCM problem for several LPOs, exploiting simple dynamical systems concepts, has shown that two TCMs provide sufficient degrees of freedom.[17] Thus, two TCMs are scheduled to occur during the transfer along the stable manifold in order to compensate trajectory deviations related to control and dynamics uncertainties. In order to correctly estimate their magnitude an OD phase is foreseen before each TCM, with the first allocated just after the SMIM and the second one scheduled to start after 6 days. Nominally, the first maneuver has to occur at least two days after the SMIM, while the second 8 days after Δv_{SMIM}. The maneuver time is selected in order to give enough time at the ground segment to perform orbit determination, compute correction maneuvers and send commands to the spacecraft. Indeed, at least one day for the OD and one day cut-off time between the end of the OD phase and the application of the TCM should be considered in order to be compliant with ESOC guidelines. A timeline for the transfer phase is given in Figure 5. Usually, the nominal trajectory does not have impulses when the correction maneuvers are applied. However, a non-null maneuver can be foreseen at each TCM time in order to broaden the feasible transfer trajectories set.
LUMIO transfer phase, as presented in Figure 5, can be subdivided into three sub-phases:

1. *OD phase* (between days 0 and 1, or between days 6 and 7 after t_0): during this phase, a visibility window is identified (see Section), and the OD algorithm is exploited within it;

2. *Cut-off phase* (between days 1 and t_{TCM_1}, or between days 7 and t_{TCM_2} after t_0): in this

phase the Differential Guidance is exploited to compute the correction maneuver, which is applied at the end of the phase;

3. *Ballistic phase* (between days t_{TCM_1} and 6, or between days t_{TCM_2} and t_f after t_0): in this phase, the spacecraft undergoes a ballistic flight.

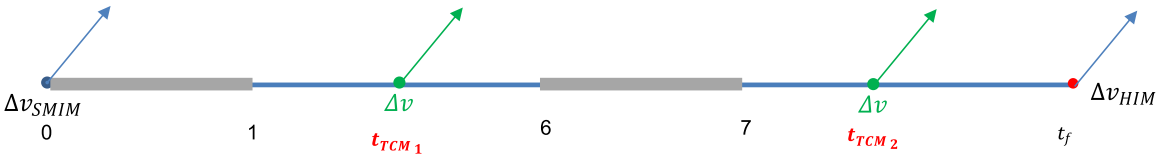

Figure 5: LUMIO transfer trajectory timeline. The grey bars represents the OD phases, while the green arrows mark the TCMs points. Time in days after the SMIM.

In this work, the transfer trajectory is the main topic and it is analyzed carefully in the remainder.

Dynamics

The motion of the CubeSat in the transfer phase can be described by using the roto-pulsating restricted n-body problem (RPRnBP),[4] in order to have a high-fidelity dynamics, able to correctly represent the highly non-linear trajectory of LUMIO. The use of an adimensional roto-pulsating frame (RPF) eases the motion description both for the transfer trajectory and for the operative orbit, since they are the generalization of trajectory existing in the restricted 3-body problem.
Equations of motion are written in a non-uniformly rotating, barycentric, adimensional reference frame with its center placed at the primaries barycenter (i.e., Earth–Moon barycenter). More details can be found in Dei Tos.[4]

Coordinates transformation The initial LLO is provided using Keplerian elements, i.e., a constant semi-major axis $a = 12\,037.1\,\mathrm{km}$ and a constant eccentricity $e = 0.65848$ plus a set of free angular parameters $\boldsymbol{\alpha}_0 = [i_0, \Omega_0, \omega_0, \theta_0]$, containing the inclination i_0, the right ascension of the ascending node Ω_0, the argument of the pericenter ω_0 and the true anomaly θ_0. Keplerian parameters are given in Moon-centered Moon-equatorial at date (MCME2000) reference frame. In this frame, the *z-axis* is aligned with the Moon's spin axis on January 01, 2000, the *x-axis* is aligned with the Earth mean equinox (First point of Aries) and *y-axis* completes the right-handed reference frame. Thus an additional transformation is needed to go from the MCME2000 Keplerian elements to the cartesian coordinates in the J2000 reference frame, before being converted in RPF. Indeed, the Keplerian elements are converted into cartesian coordinates $\mathbf{x}_{\mathrm{MCME}}$[18]

$$\mathbf{r}_{\mathrm{MCME}} = T_1 \begin{bmatrix} \frac{p\cos\theta_0}{1+e\cos\theta_0} \\ \frac{p\sin\theta_0}{1+e\cos\theta_0} \\ 0 \end{bmatrix}, \qquad \mathbf{v}_{\mathrm{MCME}} = T_1 \begin{bmatrix} -\sqrt{\frac{\mu_M}{p}}\sin\theta_0 \\ \sqrt{\frac{\mu_M}{p}}\left(e+\cos\theta_0\right) \\ 0 \end{bmatrix} \tag{8}$$

with $p = a\left(1+e^2\right)$ the semi-latus rectum, where the matrix $T_1 = R_z\left(\omega_0\right) R_x\left(i_0\right) R_z\left(\Omega_0\right)$ is defined through 3-dimensional rotation matrices. Then, the state is rotated in the Moon-Centered J2000

$$\mathbf{x}_{\mathrm{J2000}} = \begin{bmatrix} \mathbf{r}_{\mathrm{J2000}} \\ \mathbf{v}_{\mathrm{J2000}} \end{bmatrix} = T_2 \begin{bmatrix} \mathbf{r}_{\mathrm{MCME}} \\ \mathbf{v}_{\mathrm{MCME}} \end{bmatrix} \tag{9}$$

with

$$T_2 = \begin{bmatrix} 1 & 0 & 0 \\ 0 & \cos(i_M) & -\sin(i_M) \\ 0 & \sin(i_M) & \cos(i_M) \end{bmatrix}$$

where $i_M = 24\,\mathrm{deg}$ is the lunar axial tilt with respect the Earth's equator.[19] Eventually, the position on the LLO is written in the solar barycentric J2000 by translation of the center from the Moon to the Solar System Baricenter, i.e.

$$\mathbf{x}_0 = \mathbf{x}_{\mathrm{J2000}} + \mathbf{x}_M \tag{10}$$

Then, the J2000 initial state $\mathbf{x}_0$ is converted in the RPF one $\boldsymbol{\chi}_0$. The SMIM is applied on top of this initial state.

Uncertainty

In this test case, uncertainties are considered to be related only to the navigation and command errors. Errors generated by uncertainties in the dynamic model (e.g., solar radiation pressure or residual accelerations) affect the transfer trajectory to a limit extent, due to the short-time propagation, and are dominated by the other errors. Thus, they are not considered in the model.
Navigation errors are taken into account as measurement model deviations in the OD phase and through an imperfect state knowledge at the initial time. The latter leads the initial state to be modeled as a Gaussian random variable with mean as the nominal initial state, i.e.

$$\boldsymbol{\chi}(t_0) \sim \mathcal{N}\left(\boldsymbol{\chi}_0, P_{\boldsymbol{\chi}}\right) \tag{11}$$

where $P_{\boldsymbol{\chi}} = \mathrm{diag}\left(\left[\sigma_{\boldsymbol{\rho}}^2 I_3,\, \sigma_{\boldsymbol{\nu}}^2 I_3\right]\right)$ is the 6-dimensional diagonal covariance matrix, with $\sigma_{\boldsymbol{\rho}}^2$ and $\sigma_{\boldsymbol{\nu}}^2$, the initial position and velocity covariances respectively.
Command actuation errors in the nominal impulses are considered, while TCMs are assumed free from uncertainties. Since uncertainty in the HIM does not affect the transfer phase and can be compensated with the station keeping algorithm foreseen in the operative orbit, the only significant uncertain maneuver is the SMIM. Thrust magnitude and direction are both modeled as Gaussian variables with a standard deviations $\sigma_{\Delta v}$ in magnitude and σ_δ in pointing angle. The magnitude error is defined as a fraction of the nominal value, i.e., $\sigma_{\Delta v} = u\Delta v_{\mathrm{SMIM}}$, with $u \ll 1$. The covariance matrix computation for the uncertainty on the SMIM requires retrieving SMIM vector in spherical coordinates, thus

$$\Delta v = \sqrt{\Delta v_x^2 + \Delta v_y^2 + \Delta v_z^2} \tag{12a}$$

$$\alpha = \mathrm{atan2}\left(\Delta v_y, \Delta v_x\right) \tag{12b}$$

$$\epsilon = \mathrm{atan2}\left(\Delta v_z, \sqrt{\Delta v_x^2 + \Delta v_y^2}\right) \tag{12c}$$

where Δv is the magnitude, and α and ϵ are the Azimuth and Elevation respectively. Then, the associated spherical covariance, i.e. $P_{\Delta v}^s = \mathrm{diag}\left(\sigma_{\Delta v}^2, \sigma_\delta^2, \sigma_\delta^2\right)$, is transformed in Cartesian coordinates

$$P_{\Delta v} = J P_{\Delta v}^s J^T \tag{13}$$

with J the Jacobian matrix of the cartesian-to-spherical conversion

$$J = \begin{bmatrix} \cos\epsilon\cos\alpha & -\Delta v\cos\epsilon\sin\alpha & -\Delta v\sin\epsilon\cos\alpha \\ \cos\epsilon\sin\alpha & \Delta v\cos\epsilon\cos\alpha & -\Delta v\sin\epsilon\sin\alpha \\ \sin\epsilon & 0 & \Delta v\cos\epsilon \end{bmatrix} \tag{14}$$

The total initial covariance can be computed as a combination of the initial state error, plus the maneuver error

$$P_0 = P_{\boldsymbol{\chi}} + \begin{bmatrix} 0_3 & 0_3 \\ 0_3 & P_{\Delta v} \end{bmatrix} \tag{15}$$

In doing so, the number of random variables can be reduced from 9, i.e., the 6-dimensional initial state plus the 3 SMIM components, to only 6 stochastic states, reducing the probabilistic space. Characteristics of the random variables are reported in Table 1.

Table 1: Stochastic characteristics of system uncertainty.

σ_ρ [km]	σ_ν [m/s]	$\sigma_{\Delta v}$ [%]	σ_δ [deg]
1	0.01	1	1

METHODOLOGY

In order to deal with the revised approach for the LUMIO transfer phase case, a proper methodology should be devised, taking into account its peculiarities. It is of paramount importance to clarify: i) which is the method used for the uncertainty propagation and how stcohastic variables are estimated, ii) how the trajectory correction maneuver are computed, iii) and how the orbit determination is performed. Moreover, the simplifying assumptions are presented as a preliminary for the optimization problem statement.

Uncertainty propagation

Polynomial Chaos Expansion in its non-intrusive fashion is used to propagate the uncertainties. Polynomial Chaos Expansion (PCE) is a nonlinear technique, in which the input uncertainties and the solution are approximated using a series expansion based on some orthogonal polynomials, thus the approximated solution can be written as[20]

$$\hat{\mathbf{x}}(t, \boldsymbol{\xi}) = \sum_{\boldsymbol{\alpha} \in \Lambda_{p,d}} \mathbf{c}_{\boldsymbol{\alpha}}(t) \psi_{\boldsymbol{\alpha}}(\boldsymbol{\xi}) \tag{16}$$

where $\Lambda_{p,d}$ is a set of the multi-index of size d and order p defined on nonnegative integers, $\boldsymbol{\xi} = [\xi_1, \ldots, \xi_d]$ is the set of input random variables, in which each element ξ_i is an independent identically distributed variable. The basis functions $\{\psi_{\boldsymbol{\alpha}}(\boldsymbol{\xi})\}$ are multidimensional spectral polynomials, orthonormal with respect to the joint probability measure $\rho(\boldsymbol{\xi})$ of the vector $\boldsymbol{\xi}$

$$\int_{\Gamma^d} \psi_{\boldsymbol{\alpha}}(\boldsymbol{\xi}) \psi_{\boldsymbol{\beta}}(\boldsymbol{\xi}) \rho(\boldsymbol{\xi}) \, \mathrm{d}\boldsymbol{\xi} = \delta_{\boldsymbol{\alpha}\boldsymbol{\beta}} \tag{17}$$

with Γ^d representing the d-dimensional hypercube where the random variable $\boldsymbol{\xi}$ are defined and $\delta_{\boldsymbol{\alpha}\boldsymbol{\beta}}$ is the Kronecker delta function. Thus, the basis functions choice depends only on $\rho(\boldsymbol{\xi})$. For instance, Hermite polynomials are the basis for normal random variables, while Legendre orthogonal polynomials are bases for the uniform distribution.[21]
Generation of a PCE means computing the generalized Fourier coefficients $\mathbf{c}_{\boldsymbol{\alpha}}(t)$ by projection of the exact solution $\mathbf{x}(t, \boldsymbol{\xi})$ onto each basis function $\psi_{\boldsymbol{\alpha}}(\boldsymbol{\xi})$, truncated at the total order p

$$\mathbf{c}_{\boldsymbol{\alpha}}(t) = E\left[\mathbf{x}(t, \cdot) \psi_{\boldsymbol{\alpha}}(\cdot)\right] = \int_{\Gamma^d} \mathbf{x}(t, \boldsymbol{\xi}) \psi_{\boldsymbol{\alpha}}(\boldsymbol{\xi}) \rho(\boldsymbol{\xi}) \mathrm{d}\boldsymbol{\xi} \tag{18}$$

The statistics of $\mathbf{x}(t,\boldsymbol{\xi})$ can be approximated by those of $\hat{\mathbf{x}}(t,\boldsymbol{\xi})$ from the coefficients $\mathbf{c}_{\boldsymbol{\alpha}}(t)$.[22] In fact, the mean is given by

$$\bar{\mathbf{x}}(t) = E[\mathbf{x}(t,\cdot)] = \mathbf{c}_0(t) \tag{19}$$

because $\psi_0 = 1$ and $E[\psi_{\boldsymbol{\alpha}}] = 0$ for $\boldsymbol{\alpha} \neq \mathbf{0}$. The covariance can be computed as

$$P(t) = E\left[\left(\mathbf{x}(t,\cdot) - \bar{\mathbf{x}}(t,\cdot)\right)\left(\mathbf{x}(t,\cdot) - \bar{\mathbf{x}}(t,\cdot)\right)^T\right] = \sum_{\substack{\boldsymbol{\alpha}\in\Lambda_{p,d} \\ \boldsymbol{\alpha}\neq\mathbf{0}}} \mathbf{c}_{\boldsymbol{\alpha}}(t)\mathbf{c}_{\boldsymbol{\alpha}}^T(t) \tag{20}$$

where the orthonormality of the polynomial basis is exploited.
In order to keep low the number of collocation points needed to evaluated the stochastic integral in Eq. (18) *conjugate unscented transformation (CUT)*[23] is exploited. CUT is the natural extension of unscented transformation, but, instead of employing only sigma-points on the principal axes of the initial distribution function, it propagates sigma-points chosen on some peculiar non-principal axes, giving the possibility to correctly estimate higher order moments of stochastic integrals.[24] Thus, it can be used to efficiently compute the generalized Fourier PCE coefficients exploiting Eq. (18). So, CUT can be seen as just another way to compute the stochastic integral given in Eq. (18). This hybrid technique, using CUT to estimate PCE coefficient, is unimaginatively labeled PCE-CUT. This approach exhibits several advantages over the standard sparse grid interpolation techniques, such as positive quadrature weights and fewer quadrature points.
The use of PCE-CUT4 (i.e., PCE with CUT up to the forth order momentum) requires the propagation of 77 samples in order to compute the quantity of interest. The equivalent full grid tensor product would require $3^6 = 729$ samples, while Smolyak's grid needs 85 points. Thus a 10% saving is expected in the computational times. Moreover, the positive quadrature weights improve the numerical stability, giving more accurate and fast results.[25]
CUT4 results are computed by considering normalized Gaussian variables. If the random variables are represented by a generic multivariate Gaussian distribution with mean $\bar{\boldsymbol{\chi}}$ and covariance matrix P, the generic quadrature point $\boldsymbol{\zeta}_q$ can be retrieved by exploiting the affine transformation

$$\boldsymbol{\chi}_q = S\boldsymbol{\xi}_q + \bar{\boldsymbol{\chi}} \tag{21}$$

with S being the Cholesky decomposition of P, i.e., $P = S^T S$.

Stochastic variables estimation Once the PCE coefficients $\mathbf{c}_{\boldsymbol{\alpha}}$ at a given time τ are retrieved by means of the 4th-order CUT, the stochastic state at a given time can be estimated as (Eq. (16))

$$\boldsymbol{\chi}(\tau,\boldsymbol{\xi}) = \sum_{\boldsymbol{\alpha}\in\Lambda_{p,d}} \mathbf{c}_{\boldsymbol{\alpha}}(\tau)\psi_{\boldsymbol{\alpha}}(\boldsymbol{\xi}) \tag{22}$$

This solution is expected to be strongly non-Gaussian. For this reason, the final stochastic state and the functions depending on it cannot be described employing only mean and covariance, but the full probability density function (PDF) has to be estimated and then used to evaluate probabilities. In order to do that, kernel density estimation (KDE)[26] is used. In this technique, the surrogate model is exploited to inexpensively produce a number n of samples of the quantity of interest $q_j = q\left(\boldsymbol{\chi}(\tau,\boldsymbol{\xi}_j)\right)$, depending on n random variables $\boldsymbol{\xi}_j$, with $j = \{1,\ldots,n\}$. Then they are used to estimate the PDF as

$$\hat{\rho}\left(q\right) = \frac{1}{nh}\sum_{j=1}^{n} K\left(\frac{q-q_j}{h}\right) \tag{23}$$

where h is the bandwidth, and K is the kernel function. The kernel function is selected as the Gaussian PDF, i.e $K(z) = \frac{1}{\sqrt{2\pi}} \exp\left[-\frac{z^2}{2}\right]$. The cumulative distribution function (CDF) can be computed as

$$\hat{F}(q) = \int_{-\infty}^{q} \hat{\rho}(q)\, \mathrm{d}q = \frac{1}{n} \sum_{j=1}^{n} G\left(\frac{q - q_j}{h}\right) \tag{24}$$

where $G(q) = \int_{-\infty}^{q} G(q)\, \mathrm{d}q$. In the case of Gaussian kernel, $G(q) = \frac{1}{2}\left[1 + \mathrm{erf}\left(\frac{q}{\sqrt{2}}\right)\right]$.
The selection of the bandwidth is tricky and different algorithms exist. In this work, the *Silverman's rule of thumb*[27] is considered: the value of h is selected as the bandwidth minimizing the mean integrated squared error for a Gaussian distribution. In this case,

$$h = \left(\frac{4\hat{\sigma}^5}{3n}\right)^{\frac{1}{5}} \tag{25}$$

where $\hat{\sigma}$ is the standard deviation of the n samples. Using KDE is preferred with respect to a simple counting method, since a smooth $\mathcal{C}^\infty$-class CDF is obtained and this is helpful in the optimization.
In order to estimate the population quantiles, a similar technique called kernel quantile estimation (KQE) is employed. The quantile function is the left-continuous inverse of the CDF

$$Q(p) = \inf\{q : F(q) \leq p\} \qquad \text{with} \quad 0 \leq p \leq 1 \tag{26}$$

i.e., the function returning the threshold value of q, such that the probability variable being less than or equal to that value equals the given probability p. Using the KQE, the quantile function can be computed as[28]

$$Q(p, q) = \sum_{j=1}^{n} \frac{1}{nh} K\left[\frac{1}{h}\left(\frac{j}{n} - p\right)\right] \tilde{q}_j \tag{27}$$

where $\tilde{q}_j$, $j = \{1, \ldots n\}$ is the sorted set of q_j and K is the kernel function. The use of this linear KQE formula give the possibility to obtain reliable estimation for the desired quantile value, while having a $\mathcal{C}^\infty$-class function.

Orbit Determination process

In order to determine the spacecraft state knowledge along the transfer phase, a covariance analysis is performed and the knowledge is estimated by means of an orbit determination algorithm.
In this scenario, *radiometric tracking* is selected as navigation technique. Thus, the spacecraft state is estimated by means of radiometric data processed by a ground station. Radiometric data for range and range-rate are simulated, generating pseudo-measurements as

$$\gamma = \sqrt{\boldsymbol{\gamma}^T \boldsymbol{\gamma}}, \qquad \dot{\gamma} = \frac{\boldsymbol{\gamma}^T \boldsymbol{\eta}}{\gamma} \tag{28}$$

where γ is the range, $\dot{\gamma}$ is the range rate, $\boldsymbol{\gamma} = \mathbf{r} - \mathbf{r}_{GS}$ is the relative distance between LUMIO and the ground station, while $\boldsymbol{\eta} = \mathbf{v} - \mathbf{v}_{GS}$ is the relative velocity. The filter embedded in the orbit determination process is an *Ensemble square root filter (EnSRF)*.[29,30] This method exploits the capability of PCE to generate inexpensively huge ensembles of samples. Moreover, EnSRF does not require perturbed observations; thus, no sampling error is introduced in Kalman gain matrix, improving the accuracy of the filter.

Guidance law

In this work, *closed-loop control*, i.e., tracking the nominal trajectory, is used as control strategy. Maneuvers are computed at a prescribed time, in order to comply with on-ground segment requirements. The differential guidance (DG), a commonly used guidance method for deep-space missions,[13,31] is exploited. Under this framework, the TCM at time t_j can be computed as[13]

$$\Delta \mathbf{v}_j^s = -\left(\Phi_{rv}^T \Phi_{rv} + q\Phi_{vv}^T \Phi_{vv}\right)^{-1} \left(\Phi_{rv}^T \Phi_{rr} + q\Phi_{vv}^T \Phi_{vr}\right) \delta \mathbf{r}_j - \delta \mathbf{v}_j \tag{29}$$

where $delta\mathbf{r}_j$ and $\delta \mathbf{v}_j$ are the estimated deviations from the nominal state.

STATEMENT OF THE PROBLEM

Once the building blocks are established, Problem 1 has to be adapted to cope with the test case scenario, represented by LUMIO transfer phase and the general optimal control problem is converted into a non-linear programming problem. The optimization problem for the test case scenario under the revised approach can be stated as

Definition 2 (Fuel-Optimal Problem) *Find the initial and final time, τ_0 and τ_f, the two TCM times, τ_{TCM_1} and τ_{TCM_2}, the angular parameter vector $\boldsymbol{\alpha}_0$, the SMIM vector Δv_{SMIM}, and the nominal trajectory impulse at TCM times, $\Delta v_{\mathrm{TCM}_1}$ and $\Delta v_{\mathrm{TCM}_2}$, such that*

$$J = \sum_i \|\Delta v_i\| = \|\Delta v_{\mathrm{SMIM}}\| + \|\Delta v_{\mathrm{TCM}_1}\| + \|\Delta v_{\mathrm{TCM}_2}\| + \|\Delta v_{\mathrm{HIM}}\| + \sum_{j=1}^{2} Q(.99,\, \Delta v_j^s) \tag{30}$$

with $Q(0.99,\, \Delta v_j^s)$ representing the 99-percentile of the stochastic cost computed through Eq. (27)*, is minimized, while the state is subjected to the RnBP-RPF dynamics. The HIM is computed as*

$$\Delta v_{\mathrm{HIM}} = \boldsymbol{\nu}^* \left(\tau_f\right) - \boldsymbol{\nu}_\delta \left(\tau_f\right) \tag{31}$$

with $\boldsymbol{\nu}^*$ the nominal velocity and $\boldsymbol{\rho}_\delta$ is the target halo velocity.
The state is subjected to initial constraints

$$\begin{cases} E\left[\boldsymbol{\chi}^*(\tau_0)\right] = \hat{[\boldsymbol{\chi}}^*(\tau_0) = \boldsymbol{\chi}_0\left(\tau_0, \boldsymbol{\alpha}_0\right) + \Delta v_{\mathrm{SMIM}} \\ E\left[\left(\boldsymbol{\chi}^*(\tau_0) - \boldsymbol{\chi}_0\right)\left(\boldsymbol{\chi}^*(\tau_0) - \boldsymbol{\chi}_0\right)^T\right] = P_0 \end{cases} \tag{32}$$

and

$$E\left[\left(\boldsymbol{\chi}(\tau_0) - \boldsymbol{\chi}_0\right)\left(\boldsymbol{\chi}(\tau_0) - \boldsymbol{\chi}_0\right)^T\right] = P_0 \tag{33}$$

and a final constraint

$$c = \hat{F}_d(30\,\mathrm{km}) > 0.99 \tag{34}$$

with $d = \|\boldsymbol{\rho}\left(\tau_f\right) - \boldsymbol{\rho}_\delta\left(\tau_f\right)\|$, being a measure of the distance of the real trajectories from the halo at τ_f, where $\boldsymbol{\rho}_\delta$ is the target halo.
In order to be compliant with on-ground operation requirements, some linear constraints are added

$$2\,\mathrm{d} \leq \quad (\tau_{TCM_1} - \tau_0) \quad \leq 8\,\mathrm{d} \tag{35}$$

$$5.5\,\mathrm{d} \leq \quad (\tau_{TCM_2} - \tau_0) \quad \leq \tau_f - 3\,\mathrm{d} \tag{36}$$

The navigation costs and the final dispersion are estimated through the comprehensive navigation assessment. It means

$$\Delta v^s = \texttt{GL}\left(\boldsymbol{\chi}^*, \hat{\boldsymbol{\chi}}, \tau_{TCM}\right) \tag{37}$$

and

$$\hat{\boldsymbol{\chi}}\left(\tau_f^{OD}\right) = \texttt{OD}\left(\boldsymbol{\chi}^*, \hat{\boldsymbol{\chi}}, \tau_0^{OD}, \tau_f^{OD}\right) \tag{38}$$

with GL *and* OD *being the Differential Guidance (Eq.* (29)*) and orbit determination on the nominal trajectory respectively, $\hat{\boldsymbol{\chi}}$ is the estimated state, $\boldsymbol{\chi}$ the real state and $\boldsymbol{\chi}^*$ is the nominal state.*

The procedure used is summarized in Algorithm 1.

Table 2: Decision vector bounds. τ_0 is the first guess departure date.

	Dep. date	τ_f [d]	τ_{TCM_1} [d]	τ_{TCM_2} [d]	$\Delta v_{\mathrm{TCM_j}}$ [m/s]
Upper Bound	$\tau_0 + 7\,\mathrm{d}$	28	8	$\tau_f - 3\,\mathrm{d}$	10
Lower Bound	$\tau_0 - 7\,\mathrm{d}$	15	2	5.5	-10

Problem 2 is solved by exploiting a simple shooting technique.[32] This method is selected as the most suitable to solve the optimization problem, since i) the trajectory lasts only few days and nominally no middle correction is enforced, so low numerical noise is expected in the derivatives, ii) number of variables is strongly reduced, iii) and Algorithm 1 can be implemented easily.

RESULTS

The trajectories listed in Table 3, taken from LUMIO Phase A study, are used as first guesses for Problem 2. The NLP is solved for each of them. The average computational time for the optimization algorithm on a quad-core Intel i7 2.80 GHz processor is about 20 minutes. Since CUT samples can be propagated forward independently, the runtime can be easily reduced by exploiting parallelization on a multi-core workstation.

Results are summarized in Table 4. Surprisingly, the solution having the best deterministic value (i.e., #64) is not the one having the best performances when stochastic costs are considered, neither in the non-optimized or in the optimized case, and this can lead to an unnecessary waste of propellant mass. However, this choice will be sub-optimal when the stochastic costs are considered. Indeed, Solution #53 needs less propellant in the first guess comprehensive approach, allowing to save about 6% of fuel. This figure increases to 8% in the *optimized* solution under the integrated approach.

This feature is mainly related to have to possibility to fly a lower dispersion trajectory. Indeed, although the position dispersion (Figure 6) shows a similar trend for both Solution #53 and #64, the velocity dispersion (Figure 7) is lower when Solution #53 is considered and this helps the trajectory to have smaller navigation costs. Moreover, a final lower dispersion is beneficial since it allows to satisfy the final constraint with less effort.

The solution #53 has the minimum overall Δv both considering the first guess and the optimized trajectory. Thus, solution #53 would have been selected as the best-performing solution even in the sequential approach. However, solution #289 results show that a great improvement (about the 25%) can be obtained under the stochastic optimization. This feature indicates that, considering a different time-frame or a different operational orbit, it could be possible that the sequential and the integrated approach give different results, leading to a wrong choice of the nominal orbit if the stochastic optimization is not performed.

Algorithm 1: Integrated approach algorithm for test cast scenario

Procedure INTEGRATED APPROACH
- Define spacecraft and navigation settings;
- Define the uncertainty properties; ▷Table 1
- **Function** INITIALIZATION
  - Evaluate the initial CUT samples $\boldsymbol{\chi}_{k+1}^{q}$; ▷See Eq. (11)
  - Compute the random basis function for KDE-KQE;
- **Function** KNOWLEDGE ANALYSIS
  - Consider the nominal trajectory;
  - **for** $i = 1$ **to** n_P ▷Loop through n_P sub-phases
    - **switch** *sub-phase*
      - **case** *OD phase*
        - **Function** ORBIT DETERMINATION
          - Find the visibility windows;
          - Retrieve the n_M measurement times t_k;
          - **for** $k = 1$ **to** n_M ▷Loop through n_M meas. times
            - Get the pseudo-measurement; ▷See Eq. (28)
            - Apply the EnSRF; ▷See Sec.
            - Get estimated states from the filter;
            - Propagate the estimated state samples to t_{k+1};
          - **end**
          - Propagate the estimated samples up to t_f^{OD};
        - **Result:** Average error at each OD final time
      - **otherwise**
        - Propagate the states up to the *final sub-phase* time;
    - **end**
  - **end**
- **Result:** Kwowledge time evolution
- **Function** NAVIGATION COSTS & DISPERSION
  - **for** $i = 1$ **to** n_P ▷Loop through n_P sub-phases
    - **switch** *sub-phase*
      - **case** *Cut-off phase*
        - Propagate the CUT samples up to the TCM time;
        - Estimate the correction maneuvers $\Delta v_j^{s,q}$;
        - Apply the maneuvers to each sample;
      - **case** *OD phase*
        - Propagate the CUT samples up to the final OD time;
        - Estimate the mean error; ▷See ORBIT DETERMINATION
        - Evaluate the estimated samples;
      - **otherwise**
        - Propagate the samples up to the *final sub-phase* time;
    - **end**
  - **end**
- **Result:** Navigation cost estimate; Final dispersion

Result: Cost function (Eq. (30)); Dispersion statistic (Eq. (34))

Table 3: First guess optimal solutions whit $\Delta v \leq 120\,\mathrm{m/s}$.

#	**Departure date**	ToF [d]	Δv_{TOT} [m/s]
53	28 JAN 2024	16.62	74.00
64	30 JAN 2024	15.56	67.33
164	11 FEB 2024	16.71	83.11
289	27 FEB 2024	15.92	68.65

Table 4: Integrated approach optimal solutions. Subscript D stay for deterministic, while S is stochastic. The asterisk is used for the value after the optimization.

#	Δv_D [m/s]	Δv^0_{D+S} [m/s]	Δv^*_{D+S} [m/s]
53	74.00	102.60	100.14
64	67.33	108.8	108.75
164	83.11	111.88	111.75
289	68.65	125.47	101.91

Table 5: Solution #53 maneuvers magnitude.

Δv_{SMIM} [m/s]	Δv_{HIM} [m/s]	$Q(.99,\, \Delta v^s_1)$	$Q(.99,\, \Delta v^s_2)$	**Total [m/s]**
68.73	3.50	25.24	2.66	100.14

CONCLUSIONS

In this work, an integrated approach for preliminary mission analysis is devised. This technique has the aim to reduce the propellant mass needed to fly a trajectory by embedding in the trajectory design and optimization the navigation assessment and the associated stochastic costs directly in the preliminary mission analysis. This method can be fundamental in future space mission exploiting limited-capability small spacecraft, where high navigation costs may jeopardize the mission feasibility. In order to assess the performances against the traditional technique, the revised approach has been applied in a test case scenario, representing the transfer from a low lunar orbit to the operational halo orbit of the CubeSat LUMIO. For this scenario, a new technique, using conjugate unscented transformation to compute the polynomial chaos expansion coefficients, labeled PCE-CUT, is devised and used to propagate the uncertainties and estimate both the dispersion and the stochastic costs, while the knowledge analysis is performed by a combination of this technique with an ensemble square-root filter. This method is inserted in the optimization scheme. Four trajectories, coming from a grid search algorithm, are used as educated initial guesses. After the optimization is found that the solution with the best deterministic value is not the one with the minimum overall cost and the 8% of the propellant mass is saved by the integrated approach optimal solution.

REFERENCES

[1] W. Fehse, *Automated rendezvous and docking of spacecraft*, Vol. 16. Cambridge University Press, 2003.

[2] A. Poghosyan and A. Golkar, "CubeSat evolution: Analyzing CubeSat capabilities for conducting science missions," *Progress in Aerospace Sciences*, Vol. 88, 2017, pp. 59–83, 10.1016/j.paerosci.2016.11.002.

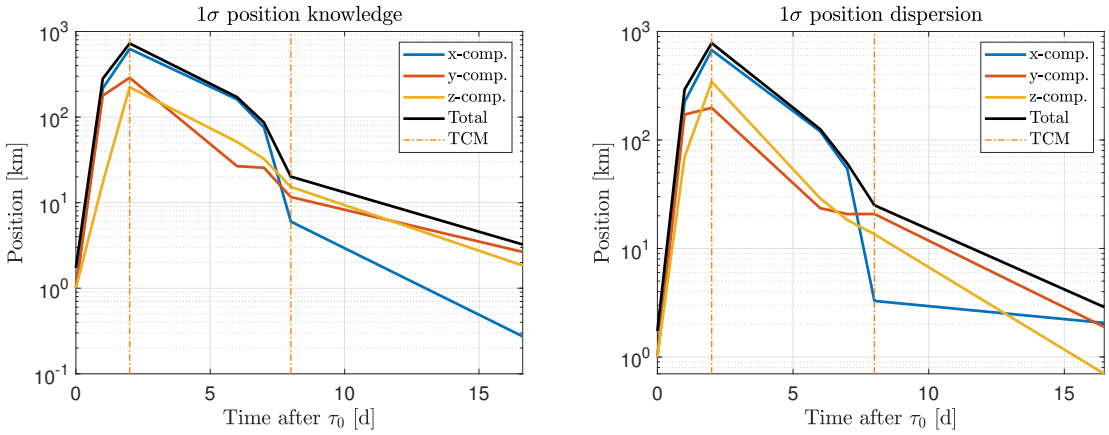

(a) (b)

Figure 6: Position 1σ dispersion evolution for the optimized cases: Trajectory (a) #53, (b) #64.

[3] R. Walker, D. Binns, C. Bramanti, M. Casasco, P. Concari, D. Izzo, D. Feili, P. Fernandez, J. G. Fernandez, P. Hager, *et al.*, "Deep-space CubeSats: thinking inside the box," *Astronomy & Geophysics*, Vol. 59, No. 5, 2018, pp. 24–30, 10.1093/astrogeo/aty232.

[4] D. A. Dei Tos and F. Topputo, "High-Fidelity Trajectory Optimization with Application to Saddle-Point Transfers," *Journal of Guidance, Control, and Dynamics*, Vol. 42, No. 6, 2019, pp. 1343–1352, 10.2514/1.G003838.

[5] A. M. Cipriano, D. A. Dei Tos, and F. Topputo, "Orbit design for LUMIO: The lunar meteoroid impacts observer," *Frontiers in Astronomy and Space Sciences*, Vol. 5, 2018, p. 29, 10.3389/fspas.2018.00029.

[6] J. M. Longuski, J. J. Guzmán, and J. E. Prussing, *Optimal Control with Aerospace Applications*. Springer, 2014.

[7] I. M. Ross, "A Historical Introduction to the Convector Mapping Principle," *Proceedings of Astrodynamics Specialists Conference*, Citeseer, 2005.

[8] R. S. Park and D. J. Scheeres, "Nonlinear mapping of Gaussian statistics: Theory and applications to spacecraft trajectory design," *Journal of Guidance, Control, and Dynamics*, Vol. 29, No. 6, 2006, pp. 1367–1375, 10.2514/1.20177.

[9] P. W. Schumacher Jr, C. Sabol, C. C. Higginson, and K. T. Alfriend, "Uncertain Lambert Problem," *Journal of Guidance, Control, and Dynamics*, Vol. 38, No. 9, 2015, pp. 1573–1584, 10.2514/1.G001019.

[10] G. Zhang, D. Zhou, D. Mortari, and M. R. Akella, "Covariance analysis of Lambert's problem via Lagrange's transfer-time formulation," *Aerospace Science and Technology*, Vol. 77, 2018, pp. 765–773, 10.1016/j.ast.2018.03.039.

[11] N. Adurthi and M. Majji, "Uncertain Lambert Problem: A Probabilistic Approach," *The Journal of the Astronautical Sciences*, Vol. 67, 2020, pp. 361–386, 10.1007/s40295-019-00205-z.

[12] C. Greco, S. Campagnola, and M. L. Vasile, "Robust Space Trajectory Design using Belief Stochastic Optimal Control," *AIAA Scitech 2020 Forum*, 2020, p. 1471, 10.2514/6.2020-1471.

[13] D. A. Dei Tos, M. Rasotto, F. Renk, and F. Topputo, "LISA Pathfinder mission extension: A feasibility analysis," *Advances in Space Research*, Vol. 63, No. 12, 2019, pp. 3863–3883, 10.1016/j.asr.2019.02.035.

[14] P. S. Maybeck, *Stochastic Models, Estimation, and Control*, Vol. 3. Academic Press, 1982.

[15] S. Speretta, A. Cervone, P. Sundaramoorthy, R. Noomen, S. Mestry, A. Cipriano, F. Topputo, J. Biggs, P. Di Lizia, M. Massari, *et al.*, "LUMIO: An Autonomous CubeSat for Lunar Exploration," *Space Operations: Inspiring Humankind's Future*, pp. 103–134, Springer, 2019, 10.1007/978-3-030-11536-4_6.

[16] F. Topputo, G. Merisio, V. Franzese, C. Giordano, M. Massari, G. Pilato, D. Labate, A. Cervone, S. Speretta, A. Menicucci, E. Turan, E. Bertels, J. Vennekens, R. Walker, and D. Koschny, "Meteoroids detection with the LUMIO lunar CubeSat," *Icarus*, 2022, p. 115213, 10.1016/j.icarus.2022.115213.

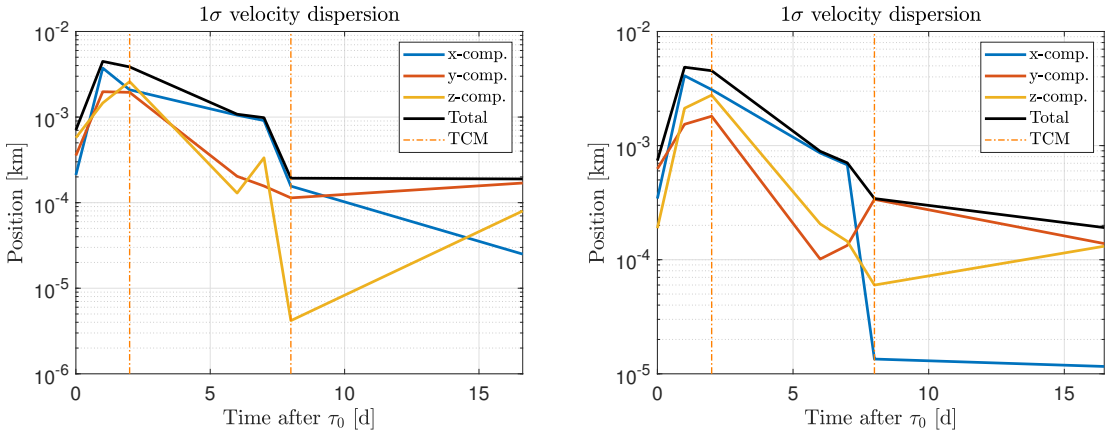

(a) (b)

Figure 7: Velocity 1σ dispersion evolution for the optimized cases: (a) Trajectory #53, (b) Trajectory #64.

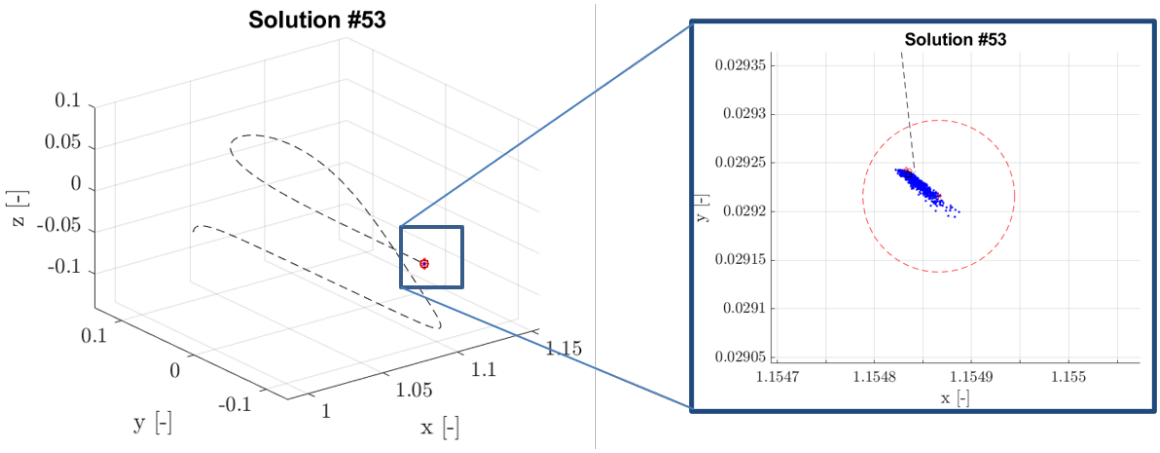

Figure 8: Transfer phase trajectory for Solution #53. In the close-up, the final dispersion is showed. The red circle represents the final constraint 30 km sphere.

[17] G. Gómez, M. Marcote, and J. J. Masdemont, "Trajectory correction manoeuvres in the transfer to libration point orbits," *Acta Astronautica*, Vol. 56, No. 7, 2005, pp. 652–669, 10.1016/j.actaastro.2004.11.005.

[18] H. D. Curtis, *Orbital Mechanics for Engineering Students*. Butterworth-Heinemann, 2013.

[19] M. W. Makemson, "Determination of selenographic positions," *The Moon*, Vol. 2, No. 3, 1971, pp. 293–308, 10.1007/BF00561882.

[20] D. Xiu, *Numerical Methods for Stochastic Computations: A Spectral Method Approach*. Princeton University Press, 2010.

[21] D. Xiu and G. E. Karniadakis, "The Wiener–Askey Polynomial Chaos for Stochastic Differential Equations," *SIAM Journal on Scientific Computing*, Vol. 24, No. 2, 2002, pp. 619–644, 10.1137/S1064827501387826.

[22] B. A. Jones, A. Doostan, and G. H. Born, "Nonlinear propagation of orbit uncertainty using Non-Intrusive Polynomial Chaos," *Journal of Guidance, Control, and Dynamics*, Vol. 36, No. 2, 2013, pp. 430–444, 10.2514/1.57599.

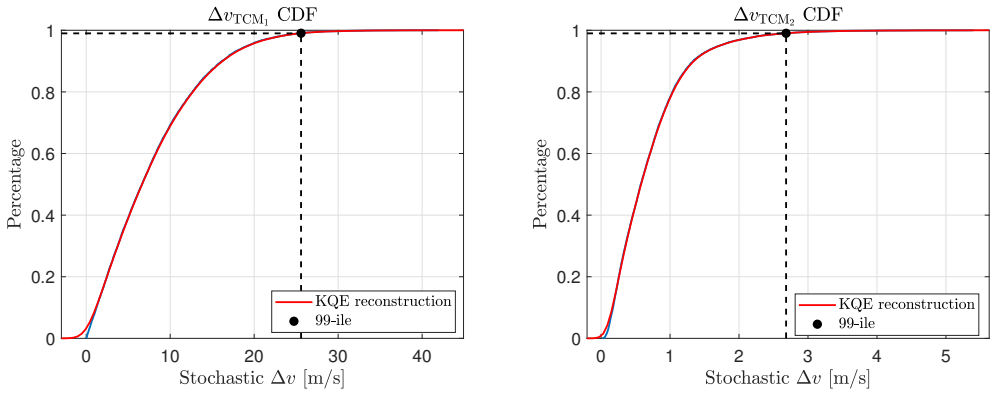

Figure 9: TCMs cumulative distribution function in Solution #53.

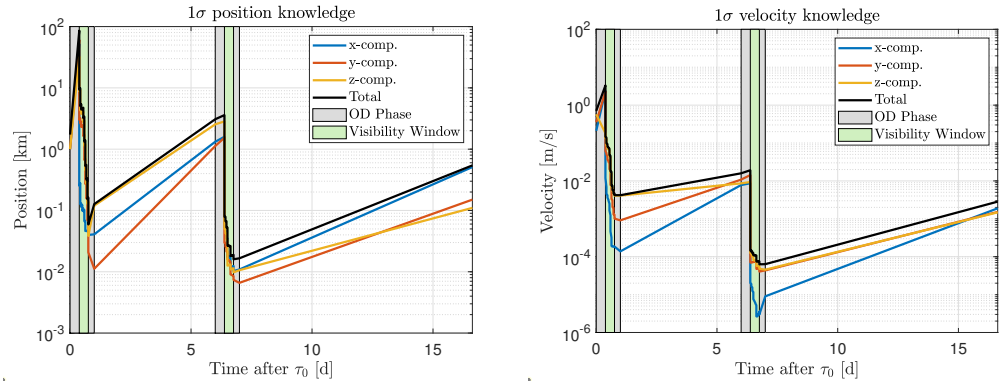

Figure 10: Knowledge analysis for Solution #53.

[23] N. Adurthi and P. Singla, "Conjugate Unscented Transformation-based Approach for Accurate Conjunction Analysis," *Journal of Guidance, Control, and Dynamics*, Vol. 38, No. 9, 2015, pp. 1642–1658, 10.2514/1.G001027.

[24] N. Adurthi, P. Singla, and T. Singh, "Conjugate Unscented Transformation: Applications to Estimation and Control," *Journal of Dynamic Systems, Measurement, and Control*, Vol. 140, No. 3, 2018, 10.1115/1.4037783.

[25] A. H. Stroud, *Approximate Calculation of Multiple Integrals*. Prentice-Hall, 1971.

[26] Z. I. Botev, J. F. Grotowski, D. P. Kroese, *et al.*, "Kernel density estimation via diffusion," *The Annals of Statistics*, Vol. 38, No. 5, 2010, pp. 2916–2957, 10.1214/10-AOS799.

[27] B. W. Silverman, *Density Estimation for Statistics and Data Analysis*, Vol. 26. CRC Press, 1986.

[28] S. J. Sheather and J. S. Marron, "Kernel Quantile Estimators," *Journal of the American Statistical Association*, Vol. 85, No. 410, 1990, pp. 410–416, 10.2307/2289777.

[29] J. S. Whitaker and T. M. Hamill, "Ensemble Data Assimilation without Perturbed Observations," *Monthly Weather Review*, Vol. 130, No. 7, 2002, pp. 1913–1924, 10/d4vdvq.

[30] J. Li and D. Xiu, "A generalized polynomial chaos based ensemble Kalman filter with high accuracy," *Journal of computational physics*, Vol. 228, No. 15, 2009, pp. 5454–5469, 10.1016/j.jcp.2009.04.029.

[31] F. L. Markley and J. L. Crassidis, *Fundamentals of Spacecraft Attitude Determination and Control*, Vol. 33. Springer, 2014.

[32] J. T. Betts, "Survey of Numerical Methods for Trajectory Optimization," *Journal of guidance, control, and dynamics*, Vol. 21, No. 2, 1998, pp. 193–207, 10.2514/2.4231.